

IV-1 Erosion of Rock and Soil

Introduction

Erosion of rock and soil (earth) are major areas of concern when dealing with earthen embankments, unlined spillways, and other features of a water control or flood risk mitigation project. Many embankment projects were not designed to be overtopped by a storm event, so any amount of overtopping flow becomes a concern. Unlined spillways are designed to experience flow and are usually expected to suffer some erosion damage; erosion becomes a dam and levee safety issue if it is so extensive that it destabilizes structures or if it enlarges or breaches through the hydraulic control section, thereby allowing an uncontrolled release of the reservoir.

When considering the many potential failure modes that include erosion of soil or rock as a necessary component, it is important to estimate not only the likelihood of erosion, but also the likelihood for various extents of erosion. Some potential failure modes that could include erosion of rock and soil as a component are:

- Overtopping erosion of an embankment
- Overtopping erosion of a concrete dam abutment or foundation
- Erosion of an unlined tunnel or spillway
- Erosion of a channel downstream of a stilling basin due to flow in excess of capacity
- Erosion of the spillway foundation where floor slabs have been damaged or lost
- Erosion of the water side slope of a levee due to riverine current or wave loading.

This chapter provides background on evaluating and estimating the erosion component of the above mentioned potential failure modes. Rather than repeat this information in a number of chapters it is provided here. The above mentioned potential failure modes have other specific considerations, such as determining the frequency and magnitude of overtopping and spillway flows and the performance of concrete linings. These elements are discussed in the individual chapters on the potential failure modes.

Key Concepts and Factors

Erosion of Embankments and Spillways

The embankments to be studied are constructed of soil, rock, or some composite of the two. This section is going to provide basic information of erosion of soil and rock for



flood overtopping and spillway flows. For details on flood overtopping and how it is handled refer to the chapter that addresses Flood Overtopping contained in this manual

Once the dam or levee has begun to overtop, or the spillway has started to flow, in general, the most erosive flow occurs on the downstream slope, as indicated in Figure IV-1-1. Velocities are normally highest on the downstream slope, and the slope itself can make it easier to dislodge and transport particles. On dams and levees that have been overtopped by floods, severe erosion has often been observed to begin where sheet flow becomes turbulent flow. Erosion can also initiate where flow encounters an obstacle or discontinuity, such as a structure, trees, shrubs, groins, bare patches of earth; or a change in embankment slope.

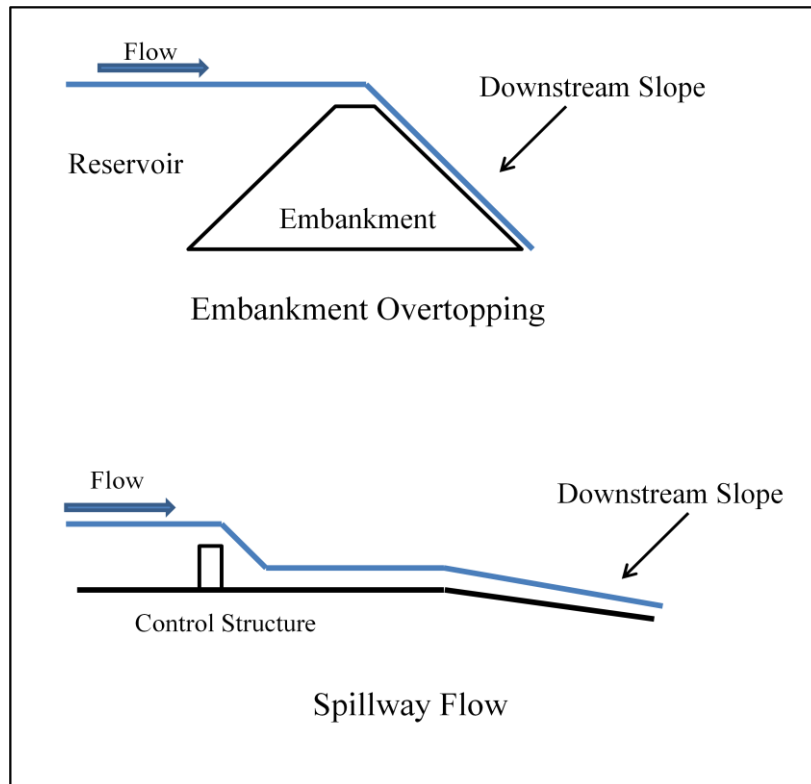


Figure IV-1-1 – Downstream Slope Locations for Embankment Overtopping and Spillway Flows

Rock Erosion

The analysis of rock erosion is a complex topic, requiring a comparison of the hydraulic attack produced by the flow and the resisting physical properties of the rock. Both can be difficult to characterize, leading to significant uncertainty. The most common approaches to the problem today rely upon technologies that were originally created for the mining and excavation of rock. Barton's Q-System (Barton 1974) was developed for

IV-1-2



the characterization of rock for tunneling activities in mines. Kirsten (1983) adapted this approach to establish a ripability index that helped the excavation industry determine the appropriate equipment needed to rip a specified rock. The primary rock properties determining the index are the joint alteration, joint roughness, joint orientation, compressive strength, and size of individual rock blocks.

The ripability index was adapted for the analysis of soil erosion and described as a headcut index by Moore et al. (1994) and Temple and Moore (1997). The index was used to establish both thresholds and rates for headcut advancement in soils. Wibowo (2005) used logical regression to develop threshold lines approximating Annandale's, but at varying probability levels.

Soil Erosion

Erosion of soil in embankments and spillways also requires a comparison of hydraulic attack and erosion resistance to determine whether erosion damage will occur and the rate at which it will progress. Multiple variables must be considered, including flow depth, shear stress, flow velocity, soil material type, geometry, armoring, and vegetation.

A dense cover of turf-type grass, as seen on many dams in the eastern U.S., can provide excellent protection against high-velocity sheet flow until the cover is removed, assuming the growth is even, and well established. When the cover is removed, or sheet flow is disrupted, concentrated flow can form initiating the headcut formation process, and all benefits of cover are lost. This is something that can be analyzed using WinDAM which is discussed later in this chapter.

Generally, the most erosion-resistant soils are plastic clays. The most erodible soils are non-plastic silts and sands. Removal of particle size is dependent on specific velocities required for transportation of various sized coarse material. For a given particle size, the slope has a major effect on the flow required to initiate erosion for cohesionless materials.

If it is necessary for the risk analysis to account for the ability of an embankment or spillway to sustain some level of erosion without failure, the analysis should begin with a consideration of whether the embankment slope protection will fail. If the downstream slope protection is cohesionless and has d_{50} larger than 4 inches, the chart from Frizell et al. (1998), Figure IV-1-2, can be used for guidance on the flow at which erosion would initiate. In the chart, S is the embankment slope (V/H), and C_u is the coefficient of uniformity (d_{60}/d_{10}), which can be taken as about 1.8 for typical clean uniform cobbles or boulders, as an initial estimate if actual values are unavailable. Note that the units are metric; one foot of overtopping corresponds to a unit discharge of roughly $2 \text{ ft}^3/\text{s}/\text{ft}$ or $0.2 \text{ m}^3/\text{s}/\text{m}$. Points plotting on the lines represent about a 20 percent probability of erosion beginning (not the probability of the dam breaching). Points plotting further below each line would indicate increasing likelihood of erosion. It is critical, however, to understand that this chart was developed from experiments on carefully placed, uniformly sized angular riprap in the ideal conditions of a straight-sided flume, not on a dam embankment with irregular groins, protruding structures, etc. that would cause local disturbance of the sheet flow. Furthermore, slope protection with an infilling of finer material may behave



differently, because much of the flow in the experiments occurred *within* the riprap, rather than over it, which may not be possible if infilling has occurred.

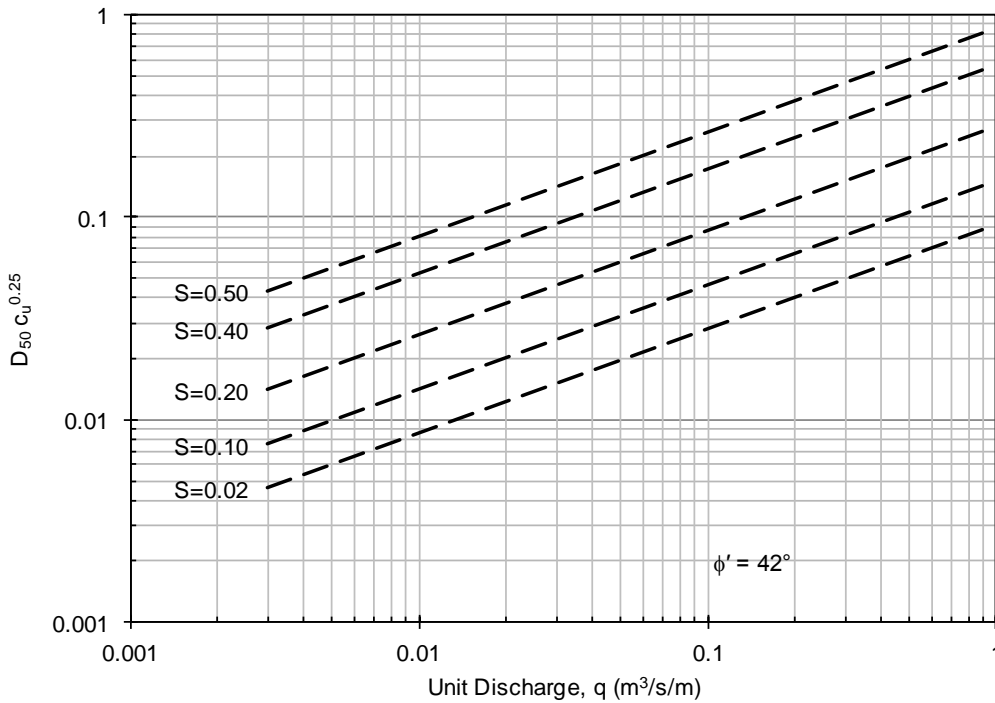


Figure IV-1-2 – Erosion Initiation Chart

Given that erosion will initiate at a specific flow depth for a system, duration should be considered as the next important variable in determining progression to the dam crest or spillway control. Once a headcut has initiated, the material properties comprising the embankment or spillway floor become important in determining the rate and extent of erosion. Erosion models presented in later sections simulate the processes of headcut formation and headcut advance that can occur after failure of the slope protection material.

When working with soil, many of the same variables are used, but they are defined differently than they are for rock. The interparticle bond shear strength (K_d) is equal to the tangent of the residual friction angle. The relative ground structure number (J_s) is always equal to one ($J_s=1$) since the material would be homogenous. The unconfined compressive shear strength (M_s) and particle size (K_b) are values that are obtained from lab data.



Shear Stress

Shear stress can be used to determine if a spillway or embankment will erode due to the water flowing across it. This calculation is also important when it is desirable to determine if flow along the toe of an embankment or in some cases levees would be events of concern. Shear stress in an open channel can be calculated using:

$$\tau_b = \gamma R_b S_e$$

Where S_e = energy slope, R_b = hydraulic radius of the bed, and γ is the unit weight of water (Chow 1964). Once the shear stress for flow in a system is known, then it is possible to compare it with the critical shear stress for a material, and a determination can be made for the erodibility of a material. This is a method that can be used for both cohesive and non-cohesive materials.

Stream Power

Although detailed hydraulic studies should be performed to estimate stream power if erosion becomes a critical issue, some simplifying conservative assumptions can be made to determine stream power for initial screening evaluations. For flow down a slope, the rate of energy dissipation per unit of surface area (P) is a function of the flow depth, flow velocity and the energy slope:

$$P = \gamma U h S$$

where γ = unit weight of water, U = flow velocity, h = water depth, and S = hydraulic energy grade line slope. The rate of energy dissipation is small as the flow just comes over the crest and increases as the water velocity increases. The analysis of erosion stability is performed at the location where the value of energy dissipation is the highest. The energy slope is assumed to be approximately equal to the bed slope and flow depths are taken to be equal to the normal depth computed for steady-state flow conditions (see Section on Overtopping of Spillway Walls).

Erodibility Index

The concept of using a rock mass index to correlate with the power it would take to remove the rock was originally developed by Kirsten (1983) to characterize the ripability of earth materials using mechanical equipment. This was extended to examine the removal of soil and rock by flowing water, and at that time the term “erodibility index” was coined. This index was correlated empirically to the erosive power of flowing water, or the energy rate of change, termed “stream power”. Data from the performance of unlined spillways in both soil and rock were used to calibrate the method for erosion potential. Thus, this method can also be used for either soil or rock, but this section focuses on its use for estimating rock erosion.

The stream power-erodibility index method can be used to estimate the likelihood of initiating rock erosion. The erodibility index (and its possible variability) represents how



erodible the foundation material is. It is relatively simple to calculate, and can be used for an initial evaluation. The stream power represents the erosive power of the overtopping flows, and is much more complicated to rigorously compute. This method will provide an indication as to the likelihood that erosion will initiate, but if so, additional judgment is needed to evaluate how quickly erosion will occur and whether it will progress to the point of initiating a failure mode (spillway breach, dam instability, dam breach). This requires evaluating the likelihood of erodibility at various depths and locations. The duration of overtopping flows should also factor into the judgment on the potential for reservoir breach.

The erodibility index, K_h , is calculated as follows:

$$K_h = M_s K_b K_d J_s$$

M_s is the mass strength, usually defined as the unconfined compressive strength (UCS) for rock (expressed in MPa) when the strength is greater than 10 MPa, and $(0.78)(UCS)^{1.05}$ when the strength is less than 10 MPa.

K_b defines the particle or fragment size of rock blocks that form the mass, which can be determined from joint spacing or rock mass classification parameters. The simplest and most straight forward relationship is $K_b = RQD/J_n$, where J_n is a modified joint set number, shown in Table IV-1-1.

K_d is the interparticle bond shear strength, and is usually taken as J_r/J_a , where J_r and J_a are the joint roughness and joint alteration numbers, based on joint surface characteristics defined by Barton's Q-system shown in Tables 15-2 and 15-3. Plucking and cyclic loading introduced by turbulence, most probably the dominant processes in scour of earth materials (Briaud, et al. 1999), act in addition to shear stress to scour earth material. Materials mainly held together by gravity bonds scour principally because of fluctuating forces developing over individual particles, as would be the case for cohesionless granular soil. The fluctuating forces pluck the soil particles out of their positions of rest. In the case of uniform cohesive soil, the cyclic loading introduced by the plucking forces weakens the soil, resulting in scour as the soil gradually yields (Colorado Department of Transportation Report No. CDOT-DTD-R-2000-9).

The relative shape and orientation of the blocks is accounted for by the J_s parameter. This represents the ease with which the water can penetrate the discontinuities and dislodge the blocks. Table IV-1-4 can be used to determine J_s .

Examples of orientation and discontinuities are shown below in Figures 15-3 and 15-4.



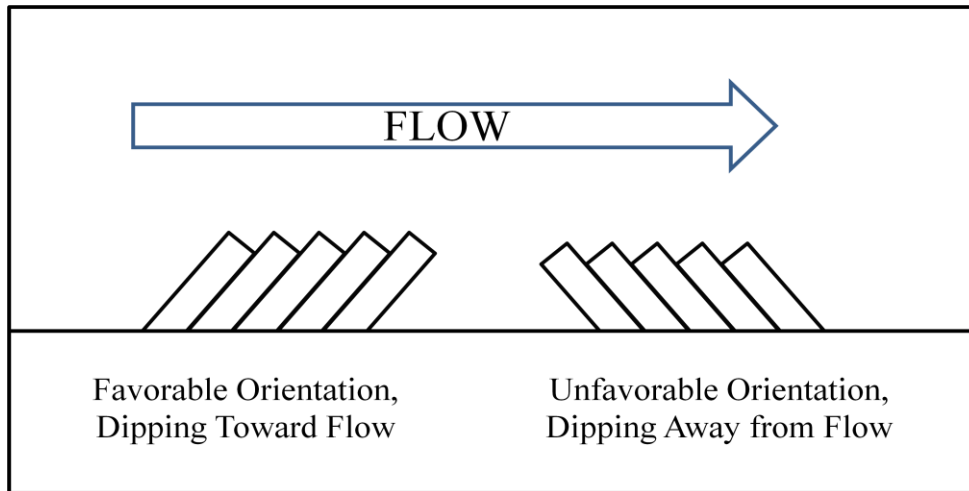


Figure IV-1-3 – Discontinuity Orientation

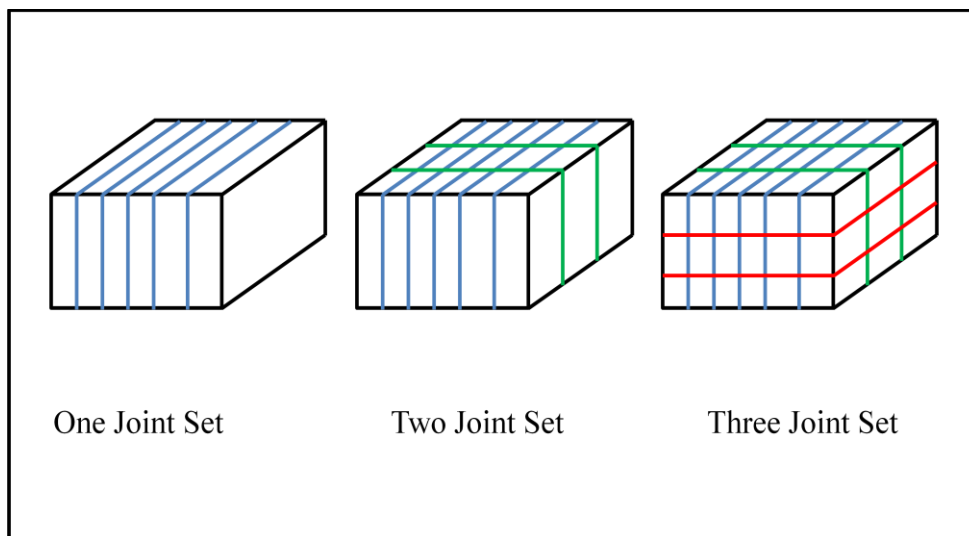


Figure IV-1-4 – Conceptual Joint Set Illustration



Table IV-1-1 – Modified Joint Set Number Values (adapted from Annandale, 2006)

Jointing Description	Modified Joint Set Number (J_n)
Intact, no or few joints	1.00
One joint set	1.22
One joint set plus random joints	1.50
Two joint sets	1.83
Two joint sets plus random joints	2.24
Three joint sets	2.73
Three joint sets plus random joints	3.34
Four joint sets	4.09
More than four joint sets	5.00

Table IV-1-2 – Joint Roughness Number (adapted from Barton, 1977)

Joint Separation	Joint Condition	Joint Roughness Number (J_r)
Tight – rock wall contact (or rock wall contact before 10 cm shear)	Discontinuous	4
	Rough or irregular, undulating	3
	Smooth, undulating	2
	Slickensided, undulating	1.5
	Rough or irregular, planar	1.5
	Smooth, planar	1.0
	Slickensided, planar	0.5
Open – no rock wall contact (even when sheared)	Clay mineral filling	1.0
	Sand, gravel, or crushed zone	1.0



Table IV-1-3 – Joint Alteration Number (adapted from Barton, 1977)

Joint Separation	Joint Condition	Joint Alteration Number (J_a)
Tight, rock wall contact	Tightly healed, hard, non-softening filling (quartz or epidote)	0.75
	Unaltered joint walls, surface staining only	1.0
	Slightly altered joint walls, non-softening mineral coatings (sandy particles)	2.0
	Silty or sandy-clay coatings (non-softening)	3.0
	Softening or low friction clay mineral coatings (< 1-2 mm thick)	4.0
Rock wall contact before 10 cm shear	Sandy particles (clay-free disintegrated rock)	4.0
	Strongly over-consolidated non-softening clay mineral fillings (< 5 mm thick)	6.0
	Clay mineral fillings, not strongly over-consolidated (<5 mm thick)	8.0
	Swelling clay fillings (< 5 mm thick, J _a increases with increasing percent of swelling clay)	8.0 – 12.0
No rock wall contact (even when sheared)	Zones or bands of silty or sandy clay (non-softening)	5.0
	Zones or bands of crushed rock and strongly over-consolidated clay	6.0
	Zones or bands of crushed rock and clay, not strongly over-consolidated	8.0
	Zones or bands of crushed rock and swelling clay fillings (J _a increases with increasing percent of swelling clay)	8.0 – 12.0
	Thick continuous zones or bands of strongly over-consolidated clay	10.0
	Thick continuous zones or bands of clay, not strongly over-consolidated	13.0
	Thick continuous zones or bands of swelling clay (J _a increases with increasing percent of swelling clay)	13.0 – 20.0



Table IV-1-4 – Determination of J_s (adapted from Annandale, 2006)

Joint Dip Angle in Flow Direction	Dips Down in Flow Direction Block Length/Thickness				Dips Up in Flow Direction Block Length/Thickness			
	1:1	1:2	1:4	1:8	1:1	1:2	1:4	1:8
0	1.14	1.09	1.05	1.02	1.14	1.09	1.05	1.02
1	1.50	1.33	1.19	1.10	0.78	0.85	0.90	0.94
5	1.39	1.23	1.09	1.01	0.73	0.79	0.84	0.88
10	1.25	1.10	0.98	0.90	0.67	0.72	0.78	0.81
20	0.84	0.77	0.71	0.67	0.56	0.62	0.66	0.69
30	0.63	0.59	0.55	0.53	0.50	0.55	0.58	0.60
40	0.53	0.49	0.46	0.45	0.49	0.52	0.55	0.57
50	0.49	0.46	0.43	0.41	0.53	0.56	0.59	0.61
60	0.50	0.46	0.42	0.40	0.63	0.68	0.71	0.73
70	0.56	0.50	0.46	0.43	0.84	0.91	0.97	1.01
80	0.67	0.60	0.55	0.52	1.26	1.41	1.53	1.61
85	0.73	0.66	0.61	0.57	1.39	1.55	1.69	1.77
89	0.78	0.71	0.65	0.61	1.50	1.68	1.82	1.91
90	1.14	1.20	1.24	1.26	1.14	1.20	1.24	1.26

Plunge Pools

When flow is concentrated into a plunge pool or at the base of a headcut, the energy dissipation rate is a function of the flow rate, the height of the drop, and the size of the jet at the impingement point. An illustration of flow overtopping a dam into a plunge pool is shown in Figure IV-1-5.



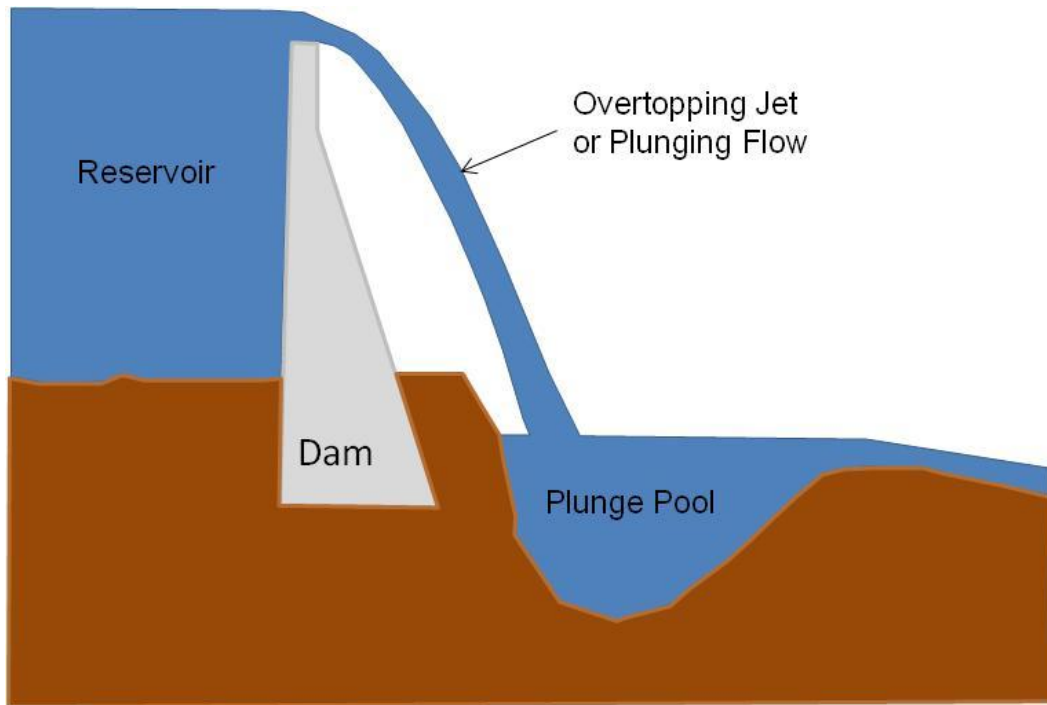


Figure IV-1-5 –Example of Plunging Flow

Equations have been proposed to predict ultimate plunge pool scour depth based on hydraulic model studies using a “moveable bed” or cohesionless sands or small gravel sizes to represent the potentially erodible material.

Equations used in the past to calculate plunge pool scour are the Veronese, Mason and Arumugam, and Yildiz and Uzucek equations. Of these equations only the Mason and Arumugam equation acknowledges that material resistance plays a role in scour. The Veronese (1937) equation is as follows.

$$Y_s = 1.90H^{0.225}q^{0.54}$$

Y_s = depth of erosion below tailwater (meters)

H = elevation difference between reservoir and tailwater (meters)

q = unit discharge ($m^3/s/m$)

Yildiz and Uzucek (1994) presents a modified version of the Veronese equation, including the angle, α , of incidence from the vertical, of the jet as follows.

$$Y_s = 1.90H^{0.225}q^{0.54}\cos\alpha$$

The Mason & Arumugam (1985) prototype equation is given as follows.

$$Y_s = K(q^x H^y h^w)/(g^v d^z)$$

h = tailwater depth above original ground surface (meters)

d = median grain size of foundation material d_{50} (meters)



$$\begin{aligned}
g &= \text{acceleration of gravity (m/s}^2\text{)} \\
K &= 6.42-3.1H^{0.10} \\
d &= 0.25\text{m} \\
v &= 0.3 \\
w &= 0.15 \\
x &= 0.6-H/300 \\
y &= 0.15+H/200 \\
z &= 0.10.
\end{aligned}$$

Unlike the Veronese and the Yildiz and Uzucek equations, the Mason and Arumugam equation includes a material factor, d . Although it is an attempt to acknowledge the role that material properties play in resisting scour, it is unlikely that this factor adequately represents the variety of material properties found in foundation materials. In addition, the materials in the movable beds of the hydraulic model studies may not scale very well to the rock material at a particular site. In most cases these equations are likely to result in a conservative estimate of maximum plunge pool scour depth, but not in all cases, particularly if the rock is likely to break into platy slabs or smaller blocks. Progression of erosion upstream also may not be realistically predicted for some rock geometries.

A jet falling any significant distance will break up to some extent while falling through the air, reducing its energy and potential for producing erosion. However, as a conservative first simplification, it can be assumed that all of the kinetic energy from an intact falling jet is dissipated on direct impact to the rock surface without any break-up of the jet, and the stream power can be estimated (in KW/m²) as

$$P = \gamma qH/d$$

where γ is the unit weight of water (9.82 KN/m³), q is the unit discharge at the location being examined (m³/s/m), H is the head or height through which the jet falls (m), and d is the thickness of the jet as it impacts the rock (m). This equation also does not account for the cushioning effects of tailwater which occurs when the jet must penetrate through the tailwater to reach the potential eroding surface (more cushioning with deeper tailwater). Thus, this produces the maximum theoretical value of streampower. In reality, the jet will begin to break up and spread out as it falls through the air. The fall height at which the jet is completely broken up can be estimated by the following equation for a circular jet (Ervine et al, 1997):

$$L_b = 1.05 \frac{D_i F_{ri}^2}{1.11 T_u^{0.82} F_{ri}^{1.64}}$$

where D_i is the thickness of the jet where it issues from the dam (typically the overtopping depth), F_{ri} is the initial Froude Number, and T_u is the Turbulence Intensity Factor from Table IV-1-5 (Bollaert, 2002).



Table IV-1-5 – Turbulence Intensity Factor (T_u) (adapted from Bollaert, 2002)

Structure Type	Turbulence Intensity Factor
Free overfall	0.00 – 0.03
Ski jump	0.03 – 0.05
Valve	0.03 – 0.08

However, the jet spread above this point can also be taken into account by the following equation (Ervine et al, 1997):

$$D = D_i + 2 * 0.38(T_u L_j)$$

where D is the jet thickness at length L_j along the jet trajectory (which can be estimated roughly or determined from a trajectory calculation). D can then be substituted for d in the stream power equation, and the stream power calculated at this point is generally assumed to remain constant for points below that level.

The above plunge pool equations can be used as a conservative first estimate of rock erosion. A more detailed stream power estimate may be appropriate if such evaluations produce a high likelihood of erosion that could lead to failure.

Erosion potential

Combining erodibility index and the stream power estimate, we can use Figure IV-1-6 to estimate the erosion potential. The green line is the initial erosion threshold proposed by Annandale (1995). Annandale (1995) reviewed about 150 field observations from spillway channels and plunge pools to develop a curve defining the threshold for erosion as a function of applied stream power and the headcut erodibility index. Based on stream power (y-axis) and headcut erodibility (x-axis) a line of best fit for the line separating cases of erosion and no erosion was determined with the reviewed datasets.



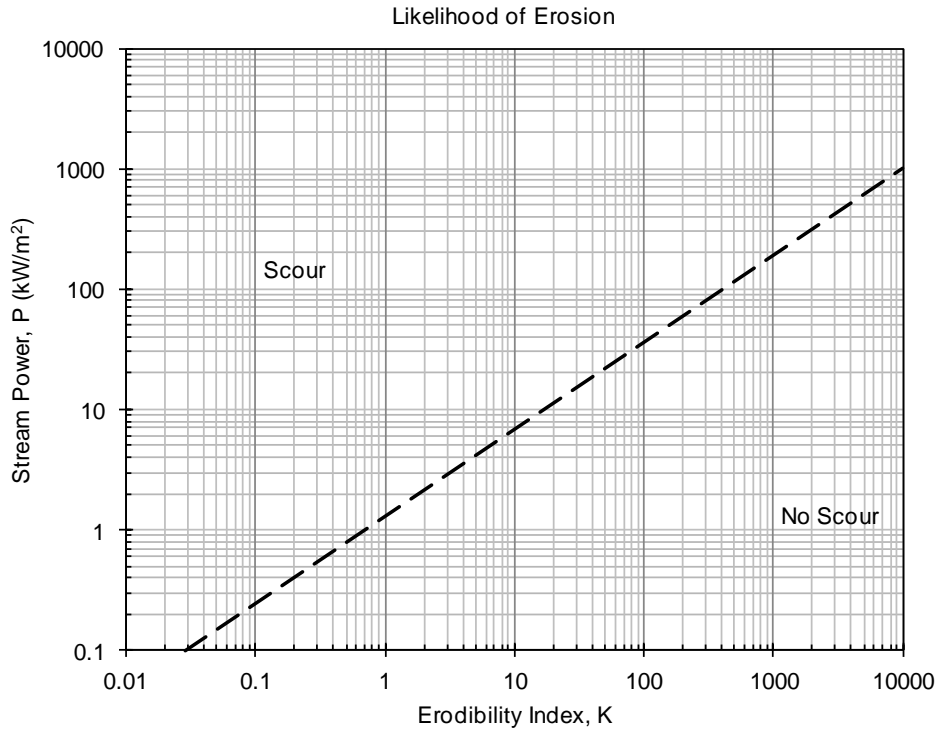


Figure IV-1-6 – Erodibility Threshold Graph (Annandale, 1995)

Figure IV-1-7 shows the logistic regression results obtained by Wibowo et al. (2005), using the same data analyzed by Annandale (1995). The upper (blue line) represents a 99 percent chance of erosion initiating. The bottom (black line) represents a 1 percent chance of erosion initiating, and the middle (red line) represents a 50 percent chance of erosion initiating. The likelihood of erosion initiation can be interpolated between these lines. If erosion is predicted, but the character of the rock or hydraulic characteristics change with depth, then an iterative procedure can be employed whereby the rock is assumed to erode to a certain depth, and then the stream power and erodibility index are recalculated for the new geometry and geologic conditions, and re-plotted on the empirical chart. Due to uncertainties in obtaining input parameters, it is often necessary to look at a range of conditions. For the analysis of a jet plunging from the crest of a concrete arch dam onto downstream canyon abutment walls, the jet will have different stream powers levels at different elevations at which it impacts the abutment.



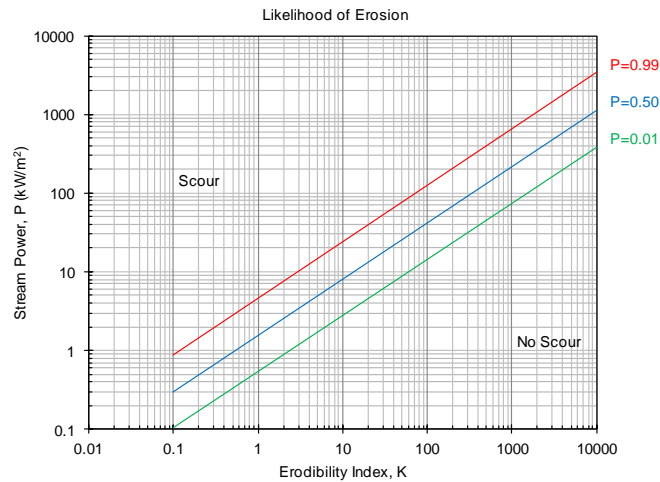


Figure IV-1-7 – Erodibility Threshold Probability Graph (Wibowo et al, 2005)

Judgment is required when applying these methods. The results can be sensitive to K_b , which is somewhat difficult to assess. In addition, materials will be more easily eroded on an abutment slope where there are more degrees of freedom for movement than in the bottom of a plunge pool where only the top of rock blocks are exposed. Cross jointing, if not present, can also increase the erosion resistance of the rock. These issues are not directly accounted for in these methods. Key block theory can be helpful in these situations to identify whether there are potentially removable blocks. A combination of the erodibility threshold graphs produced by Annandale and Wibowo can assist in providing a range when analyzing the likelihood of progression for embankment and spillway headcuts. See Figure IV-1-8 for a combined plot of the two methods.

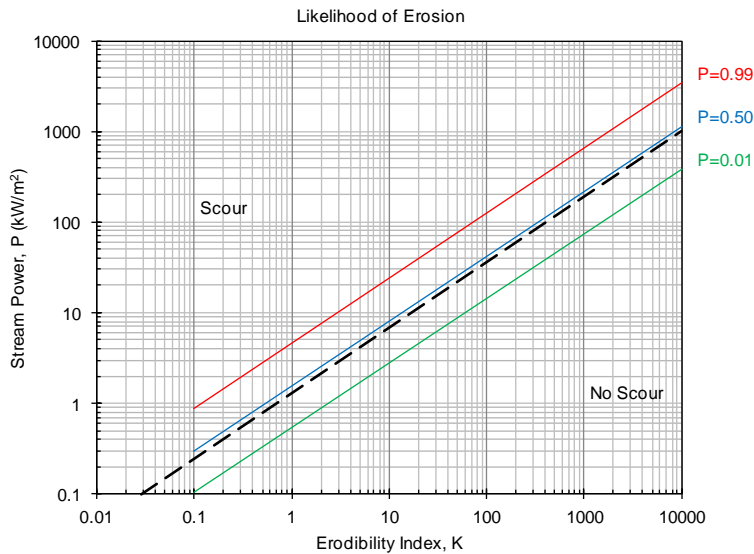


Figure IV-1-8 – Comparison of the Annandale and Wibowo Threshold Lines



Soils Parameters for Evaluating Overtopping Erosion Leading to Breach of Earthen Levees and Dams

When the hydraulic loading from overtopping, typically characterized by the hydraulic shear stress, exceeds the critical shear stress of any armoring and the underlying embankment materials, the erosion process potentially leading to breach begins. The erosion process occurs in two distinct phases, Breach Initiation and Breach Formation (Wahl 1998):

- In the breach initiation phase, the dam [*or levee*] has not yet failed, and outflow from the dam [*or levee*] is slight; outflow may consist of a slight overtopping of the dam [*or levee*] or a small flow through a developing pipe or seepage channel. During the breach initiation phase, it may be possible for the dam [*or levee*] to survive if the overtopping or seepage flow is stopped.
- During the breach formation phase, outflow and erosion are rapidly increasing, and it is unlikely that the outflow and the failure can be stopped.

For materials with some unconfined strength (sometimes loosely referred to as cohesive strength) Hanson et al (2003) has further differentiated these phases into four stages:

1. Flow over the embankment initiates at $t = t_0$. Initial overtopping flow results in sheet and rill erosion with one or more master rills developing into a series of cascading overfalls (Figure IV-1-9a). Cascading overfalls develop into a large headcut (Figure IV-1-9b and 15-9c). This stage ends with the formation of a large headcut at the downstream crest and the width of erosion approximately equal to the width of flow at the downstream crest at $t = t_1$,
2. The headcut migrates from the downstream to the upstream edge of the embankment crest. The erosion widening occurs due to mass wasting of material from the banks of the gully. This stage ends when the headcut reaches the upstream crest at $t = t_2$ (Figure IV-1-9d),
3. The headcut migrates into the reservoir lowering of the crest occurs during this stage and ends when downward erosion has virtually stopped at $t = t_3$ (Figure IV-1-9e). Because of the small reservoir size, the peak discharge and primary water surface lowering occurred during this stage, and
4. During this stage breach widening occurs and the reservoir drains through the breach area (Figure IV-1-9f). In larger reservoirs, the peak discharge and primary water surface lowering would occur during this stage ($t_3 < t < t_4$) rather than during stage III. This stage may be broken into two stages for larger reservoirs depending on the upstream head through the breach.





Figure IV-1-9 – Generalized description of observed erosion processes during ARS overtopping tests: a) rills and cascade of small overfalls during Stage I, b) consolidation of small overfalls during Stage I, c) headcut at downstream crest, transition from Stage I to Stage II, d) headcut at upstream crest, and e) transition from Stage III to Stage IV at breach formation (Hanson et al 2003).

During each of these stages, hydraulic loading exceeds the erosion resistance of the embankment soils, causing erosion. Generally it is believed that the rate of erosion is proportional to the magnitude of the applied hydraulic shear stress and the erodibility of the embankment or foundation material. For embankments and spillways comprised of highly erodible materials, relatively minor overtopping flows (say on the order of 6 inches to 1 or 2 feet) can result in high erosion rates and rapid progression of breach initiation and formation to complete breach. For these conditions, advanced erosion rate models may not be warranted and typical simplified breach formation regression relationships can be used to estimate breach formation time and peak outflow (e.g.,



MacDonald Langridge-Monopolis, 1984). For embankments comprised of moderate to high erosion resistant materials, while erosion will likely occur, the rate of erosion may be slow enough that the breach process may not progress beyond the breach initiation phase; A full breach may not develop (Briaud, 2008), significantly reducing breach outflow, inundation areas, depths and associated consequences. Thus the erodibility of the material is a primary factor impacting both the likelihood of breach and associated consequences and can affect estimates of average annual life loss (i.e., risk) by several orders of magnitude.

Empirical Correlations For Estimating Soil Erosion Rate Parameters

Several erosion studies have been performed that focus on identifying the erosion parameters and correlating those parameters to formulate an expression for erosion rates as functions of the hydraulic stress and soil erosion resistance (Hanson et al, 2011):

$$\dot{\epsilon} = k_d (\tau - \tau_c)$$

where

$\dot{\epsilon}$ = the erosion rate,

k_d = a detachment rate/erodibility coefficient (typically expressed in US units of ft³/lb-hr),

τ = the hydraulically applied boundary stress (typically in US units of lb/ft²), and

τ_c = the critical stress required to initiate erosion (typically in US units of lb/ft²).

This equation has been used in algorithms relating key processes of embankment erosion including headcut jet impingement, headcut migration, and embankment breach widening. The detachment rate coefficient k_d and critical stress τ_c are properties of the soil material and are affected by various factors including soil composition, compaction characteristics, degree of cementation, etc.... This same empirical relationship is also used in concentrated leak internal erosion analyses, where the factor of safety for initiation of pipe enlargement is related to τ_c and rate of pipe enlargement is related to k_d . In the United States, efforts by research hydraulic and geotechnical engineers have been progressing somewhat independently and for this guidance document will be characterized in an oversimplified manner as the work by the US Department of Agriculture (USDA) Natural Resources and Conservation Service and the Agricultural Research Service (“Hanson”) and the work at Texas A&M University (“Briaud”).

In Hanson and Simon (2001), results from a study to measure the erosion resistance of streambed materials in the loess areas of the midwestern USA were presented in a summary chart which included a five level characterization scheme for describing the erosion resistance of a material based on associated values of k_d and τ_c (Figure IV-1-10). k_d and τ_c were found to be loosely correlated and inversely proportional. In breach analysis, the parameter k_d is found to be the dominant parameter affecting erosion rate, thus from Figure IV-1-10, erodibility of the material is loosely characterized as follows:

Table IV-1-6

Erodibility	k_d (cm³/N-s)	k_d (ft³/lb-hr)
Very Erodible	1 to 5 (or more)	0.5 to 2 (or more)
Erodible	0.05 to 2	0.02 to 1
Moderately Resistant	0.01 to 0.5	0.005 to 0.2

IV-1-18



Resistant	0.001 to 0.4	0.0005 to 0.2
Very Resistant	0.0005 (or less) to 0.1	0.0002 (or less) to 0.1

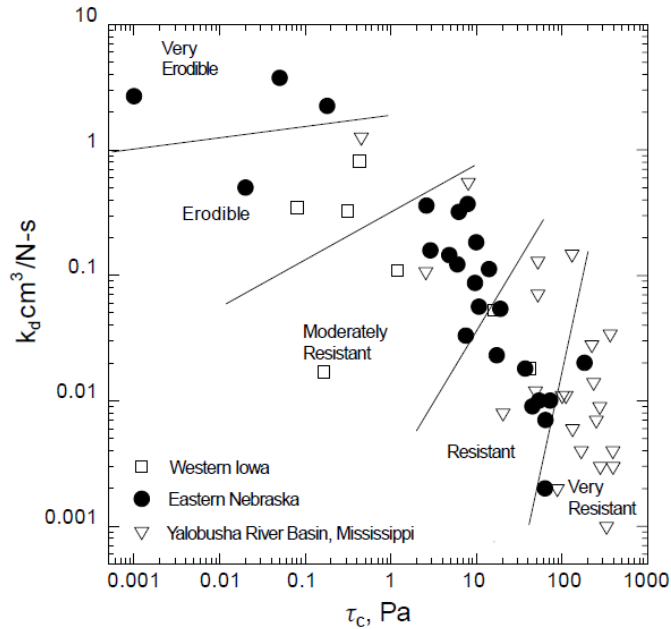
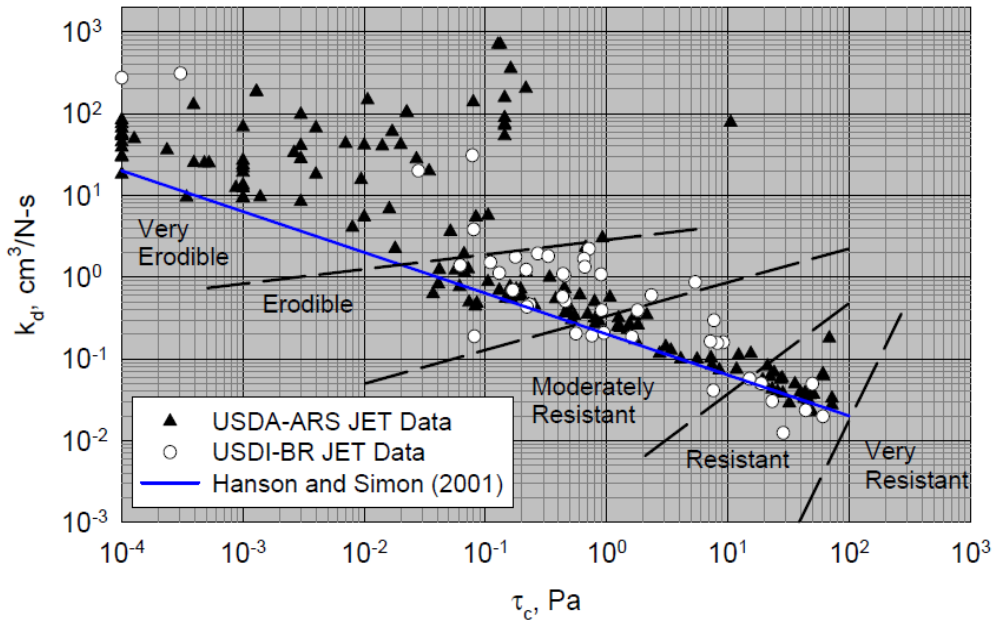


Figure IV-1-10 - τ_c versus k_d from cohesive streambed submerged JET tests (Hanson and Simon 2001)

This characterization scheme has been carried forward in joint research by the USDA Agricultural Research Service (USDA ARS) and the US Department of Interior Bureau of Reclamation (USBR), such as in Figure IV-1-11 (Hanson et al, 2010).



IV-1-19



Figure IV-1-11 - Relationship of k_d and τ_c from JET tests on soil at the USDA-ARS Hydraulic Engineering Research Unit and USBR Hydraulic Laboratory (Hanson et al, 2010)

In Simon et al (2010), data from erosion tests on stream deposits suggested a similar relationship between k_d and τ_c with the relationship being influenced by test device and generally shifted up and to the right for the presumably uncompacted and less erosion resistant natural sediments (Figure IV-1-12).

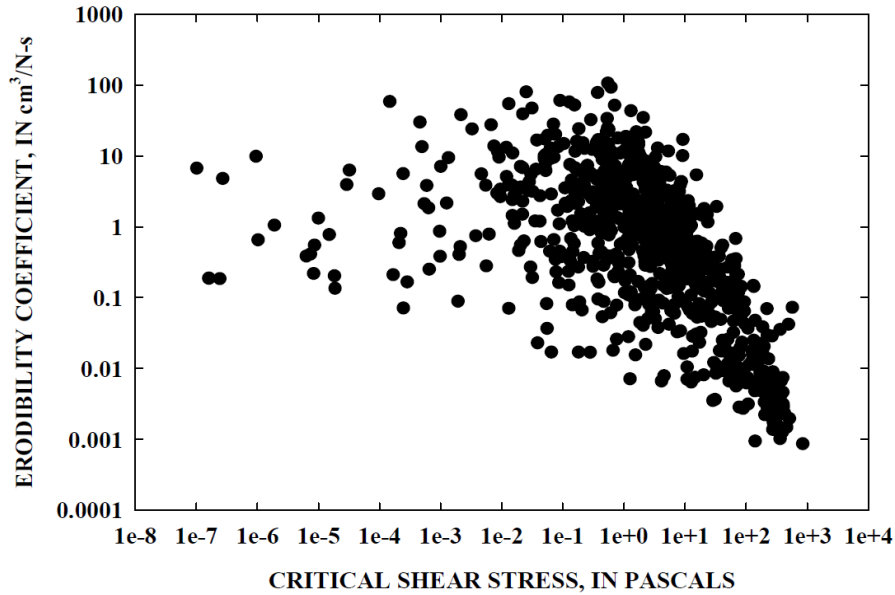


Figure IV-1-12 - Relationship of k_d and τ_c from 775 JET and Mini-Jet tests on natural sediments (Simon et al, 2010)

In Briaud et al (2001), a new test device, the Erosion Function Apparatus (EFA) is described and results from tests on various soils are presented. In a companion discussion, Hanson and Simon (2002) plot the Briaud et al (2001) data on the Hanson and Simon (2001) erodibility classification scheme (Figure IV-1-13), again showing a similarly correlated relationship between k_d and τ_c .



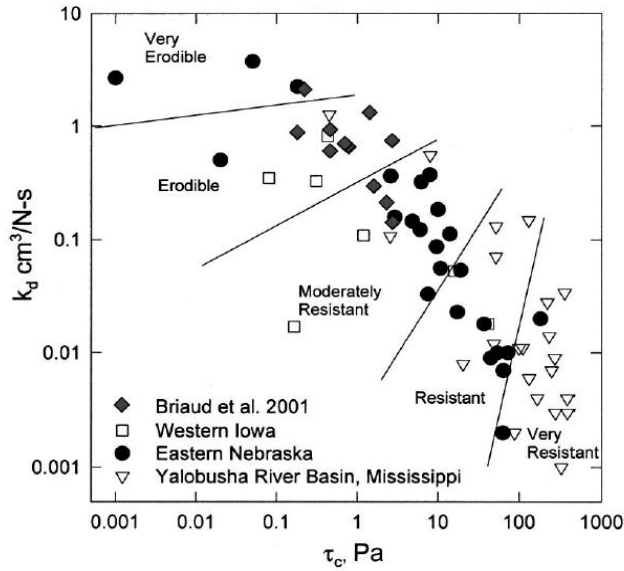


Figure IV-1-13 Briaud et al (2001) Erosion Function Apparatus test results plotted on Hanson and Simon erodibility classification chart (Hanson and Simon 2002)

In Briaud et al (2008), results from a study to evaluate the erodibility of levees overtopped during hurricane Katrina were presented in a summary chart which included a new six level characterization scheme for describing the erodibility of a material based on associated values of flow velocity (sometimes presented as hydraulic shear stress) and erosion rate (Figure IV-1-14). In New Orleans during Hurricane Katrina overtopping, levees that had Very High to High Erodibility breached while levees that had Medium to Low Erodibility did not.



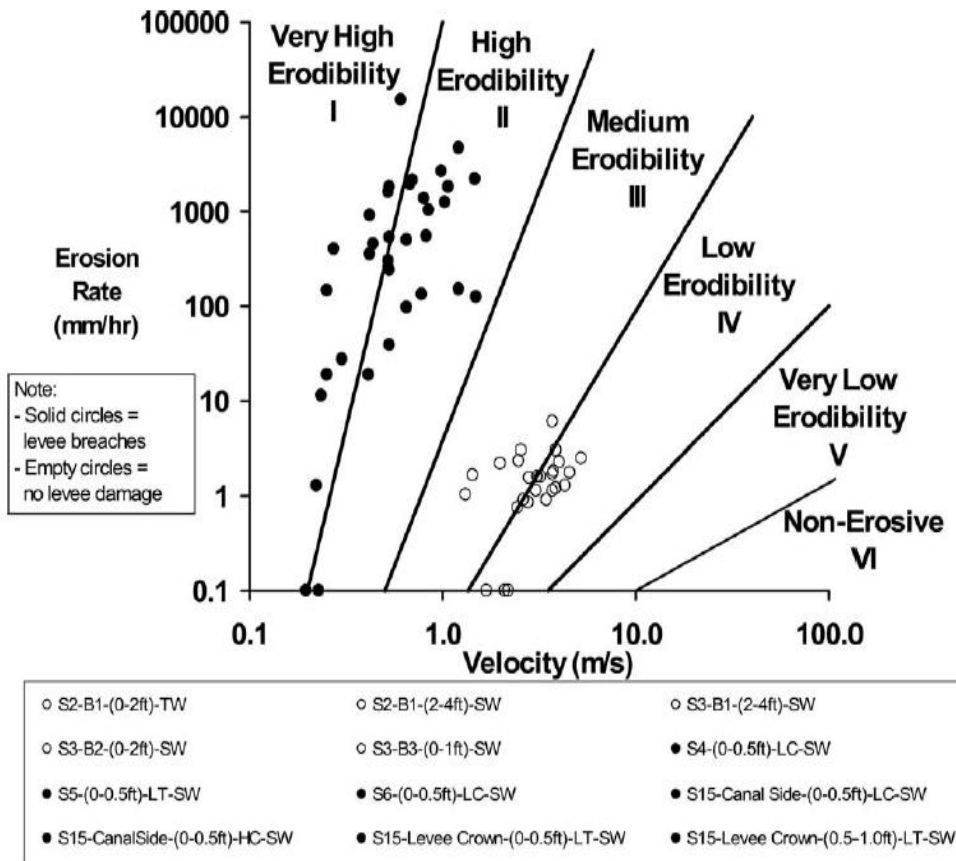


Figure IV-1-14 Erosion Function Apparatus test results and overtopping levee failure/no failure chart. Solid circles are for levees that failed and empty circles are for levees with no damage (Briaud et al 2008)

In Briaud (2008), the above erodibility characterization scheme was expanded to encompass a wider variety of materials described in general engineering terms (Unified Soil Classification System (USCS) based on % and type of coarse versus fines and the plasticity of the fines for soils and jointing characteristics for rock) rather than the agricultural “textural” terms (% sand, silt, and clay based on grain size definitions) often used in the USDA work (Figure IV-1-15).



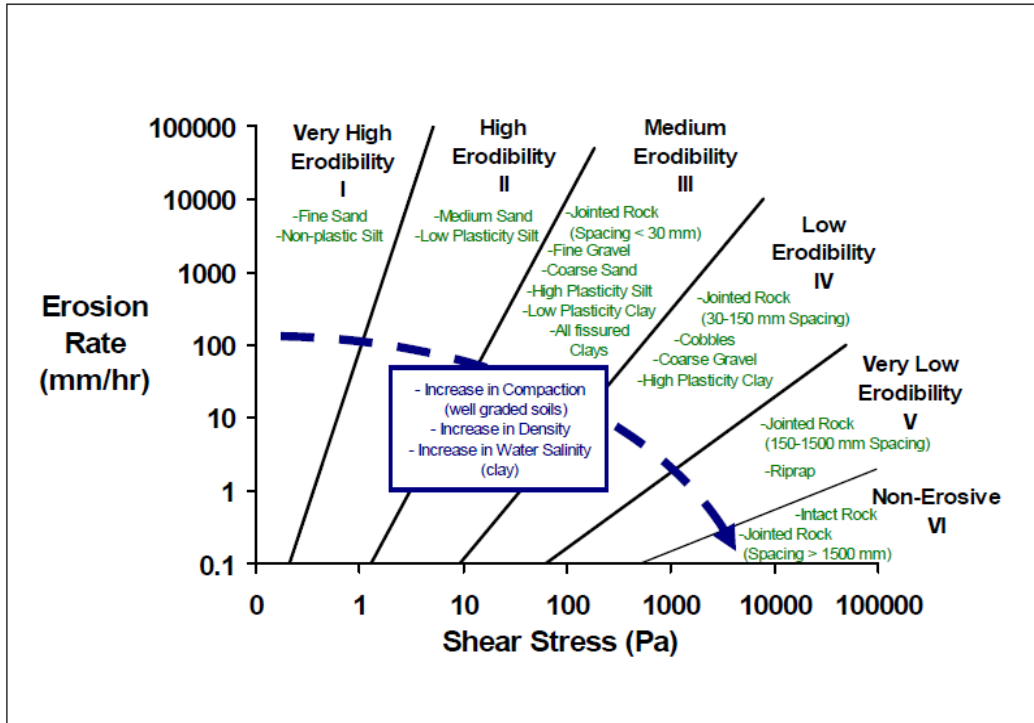


Figure IV-1-15 Proposed erosion categories for soils and rocks based on shear stress (Briaud 2008)

Briaud et al (2001) suggests that τ_c is related to mean soil grain diameter, similar to Shields (1936) (Figure IV-1-16).

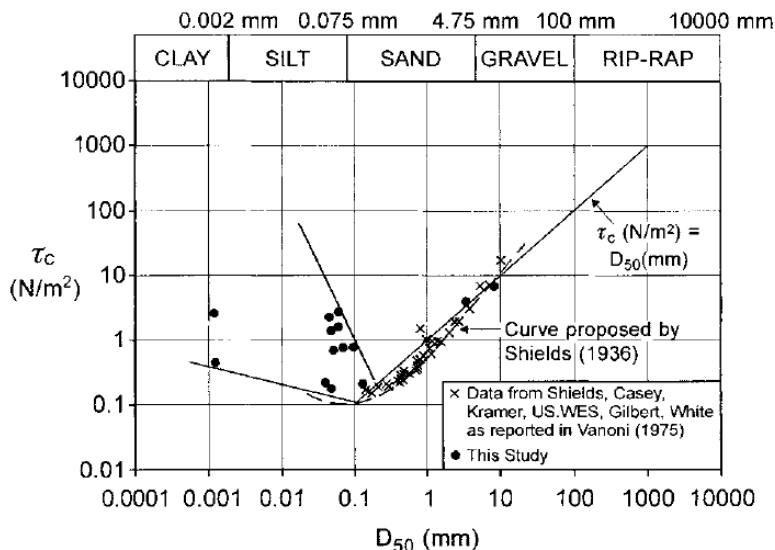


Figure IV-1-16 Critical Shear Stress versus Mean Soil Grain Diameter (Briaud et al, 2001)

Figure IV-1-17 presents an overlay of the “Hanson” erosion resistance classification (Figure IV-1-10 above), a proposed transformation of the “Briaud” erodibility classification together with Briaud associated materials (Figure IV-1-15 above), URS Levee Erosion Toolbox (URS 2007, to be discussed later) analysis default erosion



parameters and τ_c based on mean grain size, D_{50} , from Briaud 2001 (Figure IV-1-25 above). The “Hanson” and “Briaud” classification schemes appear to be complimentary, with each erosion class having similar ranges of values for k_d and associated τ_c . At this time, risk analysts are encouraged to continue using the classification scheme and nomenclature of Hanson and Simon (Figure IV-1-10 and Table IV-1-6) when describing the erosion resistance of materials.

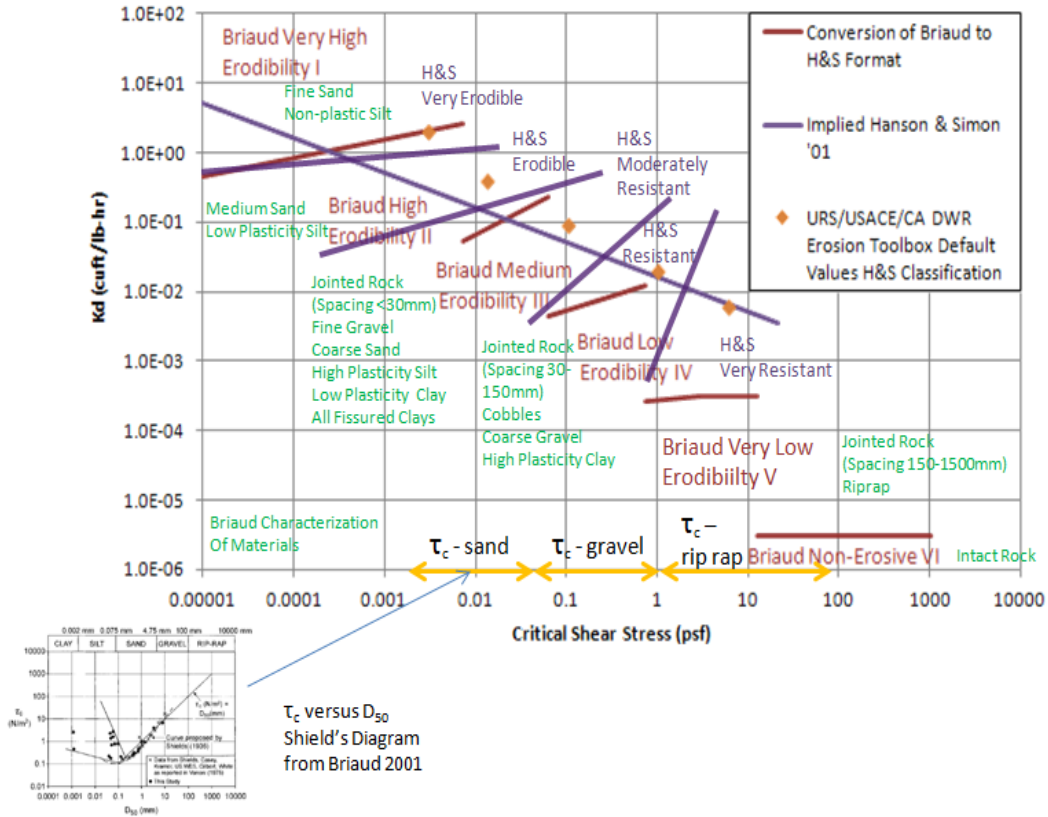


Figure IV-1-17 “Hanson” erosion resistance, “Briaud” erodibility, Levee Erosion Toolbox (URS 2007) default values for k_d and associated τ_c for the various “Hanson” erosion resistance classifications and Shield’s Diagram τ_c from Briaud 2001.

Physical Tests For Estimating Soil Erosion Rate Parameters

Several test methods have been developed for evaluating detachment rate coefficient k_d and critical stress τ_c , including: flume tests, jet erosion test (JET), rotating cylinder test (RCT), small samples inserted in the bottom of flumes (aka Erosion Function Apparatus EFA), and hole erosion test (HET) are representative examples from the literature (Hanson et al, 2011). At this time, the JET test is considered the best understood with the most confirmation of coherence between small scale test results and the larger scale erosion processes modeled in overtopping analyses. HET tests have gained some popularity for evaluating internal erosion potential (scour/crack erosion), but have been found to generally yield estimates of k_d on the order of 1 to 2 orders of magnitude too low compared to JET tests and small scale models (Wahl et al 2008). Unfortunately, available JET devices are too small to test samples of rockfill materials (e.g., coarse



sands, gravels and cobbles), which are typical materials for many dam embankment shells.

Factors Affecting Soil Erosion Rate Parameters

Hanson et al (2011) presents JET erosion test results from low plasticity clayey materials compacted at different compactive efforts and moisture contents, showing that compaction moisture content can have a significant impact on both k_d (Figure IV-1-18) and τ_c .

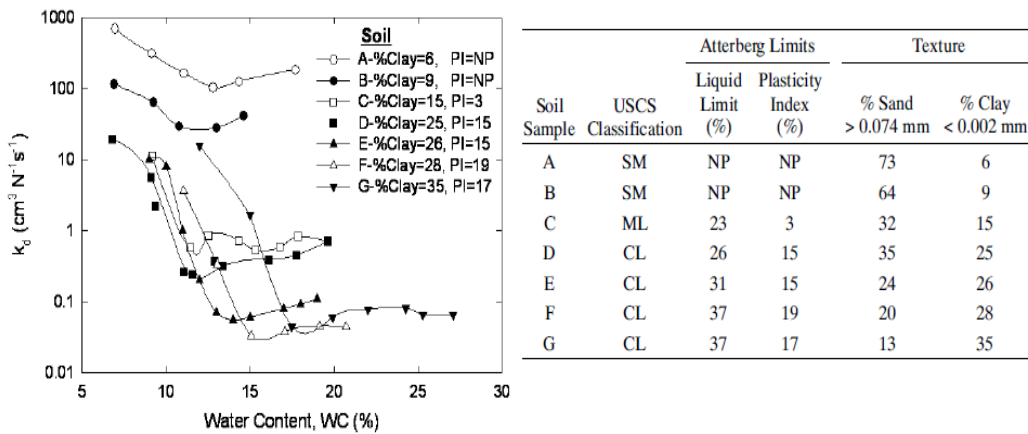


Figure 15-18 Change in k_d versus compaction water content for seven low plasticity soils compacted at Standard Proctor (ASTM D698). Lowest values of k_d are generally achieved just below or near optimum water content. (Hanson et al, 2011)

Figure IV-1-19 presents the measured values of k_d from Hanson et al (2011), indicating that for the low plasticity CL soil tested, k_d decreases with increasing compactive effort.

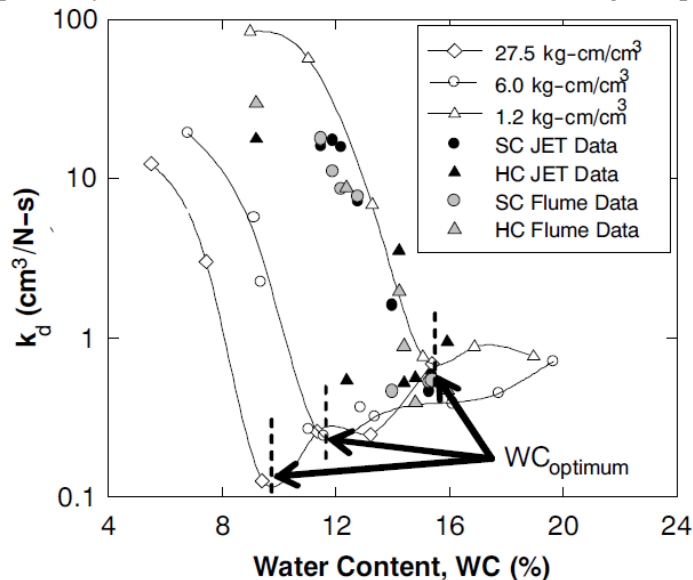
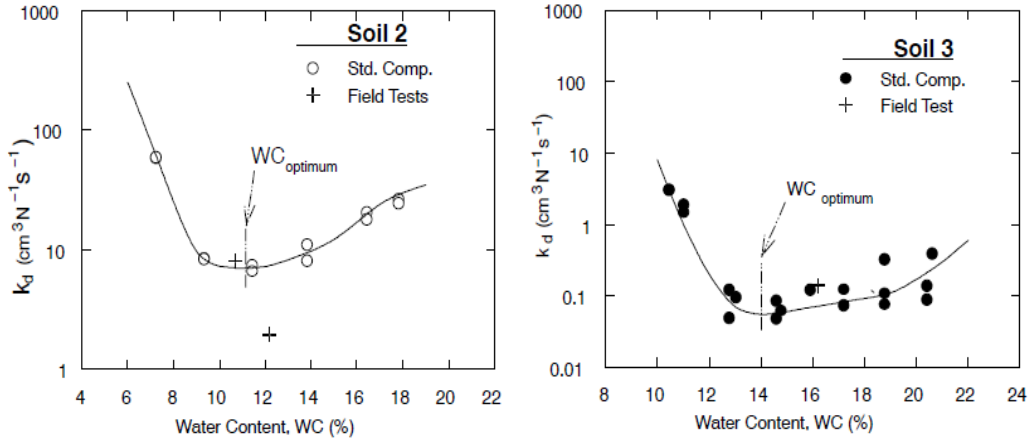


Figure IV-1-19 k_d versus Compaction Water Content for Different Compactive Efforts (low, “Standard”, and “Modified” Proctor, based on energy level in Kg-cm^3) (Hanson et al, 2011)



Figure IV-1-20 presents results from Hanson and Hunt (2007) indicating a slightly different relationship for the SM and slightly dispersive CL material tested in this study, with these materials showing less immediate increase in K_d when compacted dry of optimum. Similar results were found in Wahl et al (2009).



Soil	Grain Size ^[a]			Plasticity Index ^[b] PI	% Dispersion ^[c]	Standard Compaction ^[d]		Soil Classification ^[e]
	% Sand > 75 μm	% Fines > 2 μm	% Fines < 2 μm			γ_{dmax} ($\text{Mg}\cdot\text{m}^{-3}$)	WC_{opt} (%)	
2	63	31	6	NP ^[e]	0	1.871	11.0	SM-Silty Sand
3	25	49	26	17	20	1.779	13.9	CL-Lean Clay

Figure IV-1-20 Variation of K_d with variation in compaction moisture content (Hanson and Hunt 2007)

Figure IV-1-21 presents the measured values of k_d from Hanson et al (2010 and 2011), Wahl et al (2009) and Shewbridge et al (2010, to be discussed later), suggesting that k_d may also vary with plastic index, decreasing with increasing plasticity, consistent with the erosion classification chart of Briaud (2008). Unfortunately “paired” samples for “dry” and “wet” comparisons of higher plasticity materials are not available to confirm higher erodibility if compacted and tested with water content dry of optimum.



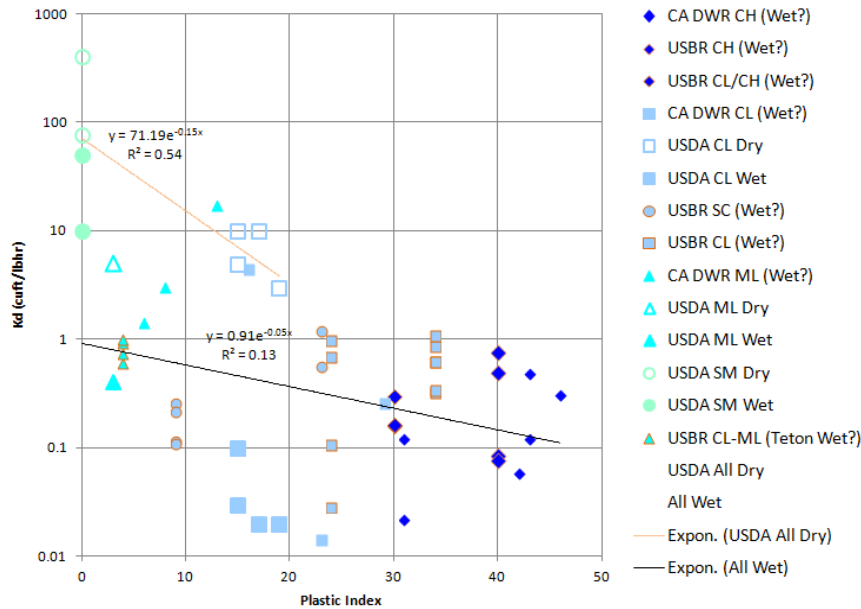


Figure IV-1-21 K_d versus Plastic Index from tests by Hanson et al (2010 and 2011) , Wahl et al (2009) and Shewbridge et al (2010).

While Briaud (2008) suggests that gravels have medium to low erodibility and thus lower expected values of k_d and τ_c , unfortunately there is no test data available at this time to confirm this supposition. Nevertheless, it seems reasonable to presume that both parameters are sensitive to the amount and type of finer grained materials comprising the gravel, as well as the inclination of the eroding surface. Steep erosion surfaces (i.e., inclined near the friction angle of the gravels), comprised of poorly graded gravels with little sand and little to no fines, might have high erodibility until the eroding surface flattens below the angle of repose as breach initiation advances. In contrast, relatively flat erosion surfaces (i.e., inclined at say 70% of the friction angle of the soil), with appreciable sand and fines (e.g., GW-GC or GC) may have very low erodibility, approaching that of jointed rock. In a review of the regression breach formation equations of Xu and Zhang (2009), Wahl (2014a) suggests that medium erodibility may be an appropriate designation for rockfill dams. Unfortunately there is little empirical evidence to support the above speculations and until more research data becomes available, the risk analyst will have to apply judgment when selecting values for k_d and τ_c to model breaches in embankments comprised of these types of materials.



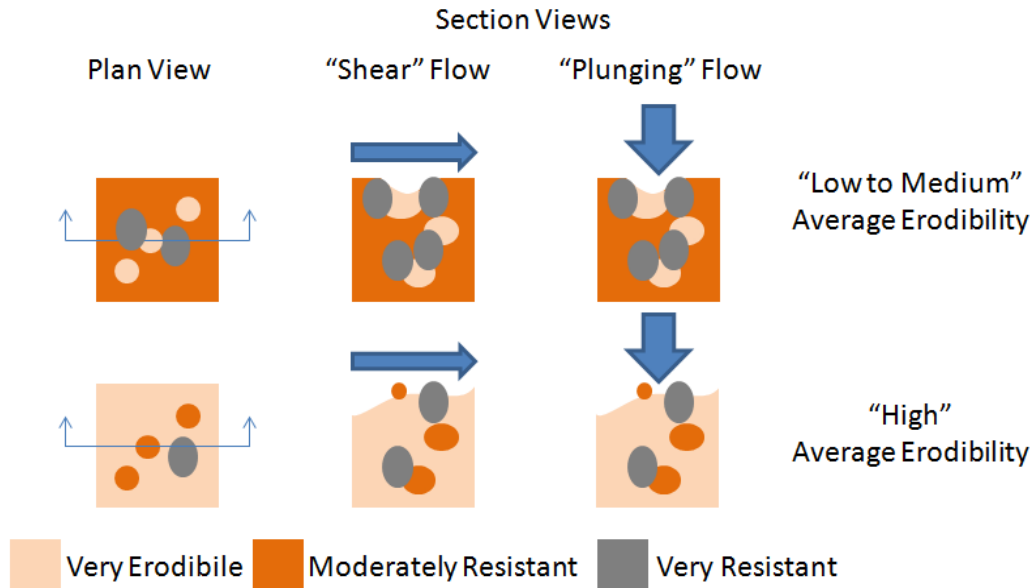


Figure IV-1-22 Material composition affects average erodibility for modeling different composite materials such as a gravelly clay (CL - upper material) and a gravelly silt (ML - lower material). Distribution and relative proportions are both important.

Estimating representative modeling values for k_d and τ_c for soils with variable constituents compacted at various water contents requires some consideration of the relative proportions, magnitudes and scales of the discontinuities. Relatively heterogeneous mixtures of low, medium and high erodibility materials may have relative low erodibility if the low and medium erodibility materials provide “protection” for the highly erodible materials. In contrast, mixtures with extensive areas of high erodibility materials may not experience any benefit from a small proportion of low erodibility materials (Figure IV-1-22) if the more erodible materials undermine the more resistant ones. Direct weighted averaging of constituent concentrations is unlikely to give appropriate estimates of average erodibility; some consideration of spatial distribution is likely necessary. Wahl (2014b) suggests that in some cases, JET testing of reconstituted samples stripped of larger erosion resistant materials (e.g., gravels) may give reasonable estimates of average properties. Again, at this time the literature does not provide complete guidance and the risk analyst must apply judgment to get a good estimate of the expected behavior. Application of design conservatism is likely not appropriate and will result in overestimates of risk, resulting in overestimation of both likelihood of failure and associated consequences, so the risk analyst is obligated to make the case to support their best estimates of parameters.

“Native” materials may also need to be considered in breach analysis and are affected by many of the same factors discussed above, but may also be affected by geologic processes that will increase or decrease the erosion resistance. In general, materials that have experienced high stresses in the past, such as glaciated foundation clays and well-consolidated claystones, will behave like materials that have been compacted under very high compactive effort, resulting in lower erodibility. Similarly, often older deposits will have some amount of natural cementation, which can impart considerable erosion



resistance, but which may also be vulnerable to degradation through solutioning water flows and/or through slaking or other wet/dry phenomena. Further, both native and engineered fill materials are subject to various processes, such as shrinking and swelling with seasonal variations in moisture; this may result in cumulative change in erosion characteristics over time, with deeper material being less and shallower material being more susceptible to those changes. Finally most erosion tests are conducted on compacted samples at the compaction water contents immediately after compaction, which may not reflect in-situ conditions. Based on limited anecdotal evidence, in some situations, it is possible that moisture conditioning over time and at relatively high confining stresses in-situ could diminish the flocculated clay structure that may form in plastic clays compacted dry of optimum, resulting in an increase in erosion resistance with time (Figure IV-1-23, Wahl 2014b and Wahl 2015). This may explain in part why undisturbed samples of saturated silts and clays retrieved from levees in California and tested in the EFA device (Shewbridge et al 2010, to be discussed below) have lower erodibility than laboratory compacted samples of many of the compacted, unsaturated silts and clays tested in the JET apparatus by USDA and USBR. Again, at this time the literature does not provide complete guidance and the risk analyst must apply judgment.

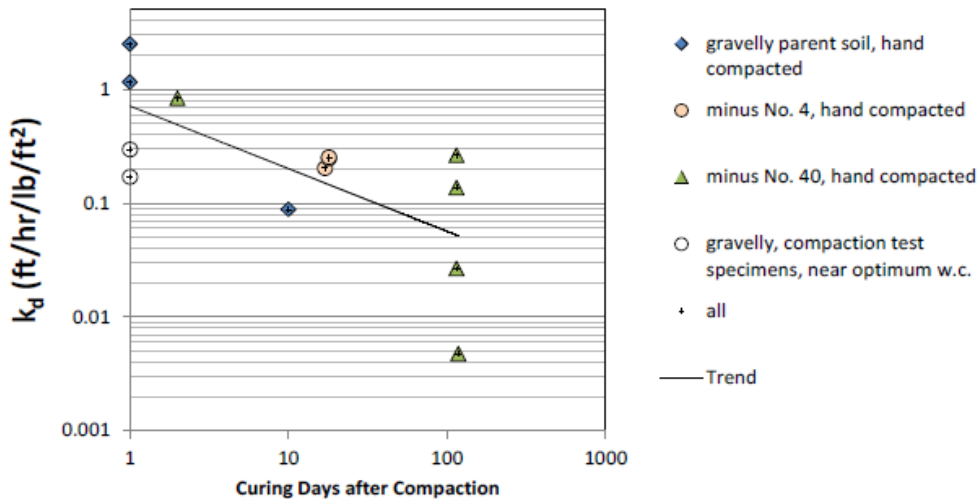


Figure IV-1-23 Jet erodibility test results versus specimen curing time after compaction.

Unconfined Strength In Headcutting Models

In most headcut erosion estimating models, an estimate of soil unconfined strength or “apparent” cohesion is also typically required and serves as a limit to the maximum height the headcut wall can achieve during erosion. In general, fine grained higher plasticity materials are more likely to exhibit unconfined strength, though most soils with some amount of sands and fines in the matrix can exhibit significant unconfined strength when partially saturated (e.g., clayey gravels). Preliminary results from breach modeling research (Morris et al 2012) indicate that advanced breaching models that incorporate a headcutting scheme can be used to model the erosion process for non-cohesive materials. In general, if using an analytical tool that models headcutting processes, when modeling breach for rockfill materials that are likely to have little to no unconfined strength, at this time it is recommended to set the unconfined strength / apparent cohesion to as small a



value as allowed and conduct sensitivity analyses to confirm the impact on final results. WinDAMB allows a minimum of 100 psf of apparent cohesion, which is a very small value leading to very short headwall heights.

Soils Parameters for Evaluating Riverine Erosion Leading to Breach of Earthen Levees

In URS 2007, a levee erosion toolbox developed for the U.S. Army Corps of Engineers (USACE) as part of the Nationwide Levee Risk Assessment Methodology project is described. The purpose of the erosion toolbox is to estimate the conditional probability of levee failure due to surface erosion on the waterside of a levee. It is a risk analysis tool for use during screening level assessments of levee risk; it is not a design tool and may reflect less conservatism than some of the design work described above. Representative “default” values for k_d and τ_c associated with the “Hanson” erosion resistance categories for use in the risk analysis computational tool were also proposed, but could be modified by the analyst, as appropriate based on site-specific material characteristics. This toolbox also suggested that typical USCS soil types could be associated with ranges of critical shear stress based on the work of Briaud (2008) (Figure IV-1-24). It must be emphasized that k_d values for large non-cohesive materials (coarse sands, gravels and cobbles) have never been measured; although the USCS soil type labels are overlaid on Figure IV-1-24 in a way that follows the relation between k_d and τ_c for cohesive materials, there is no assurance that non-cohesive materials will have similar k_d values.

In Shewbridge et al (2010), test results from a study for the California Department of Water Resources to apply the USACE erosion toolbox methodology to levees in California are presented. Undisturbed samples of actual levee materials from various locations throughout the California Central Valley were retrieved, classified per the USCS and tested in the Erosion Function Apparatus (Briaud et al, 2001). These test results suggest that the default values for k_d and τ_c as functions of “typical” soil type proposed in URS 2007 were appropriate for levee screening-level risk analyses. Low plasticity materials (silts and low plasticity clays) had higher values and higher plasticity materials (higher plasticity clays) had lower values of k_d resulting in higher and lower predicted and measured erosion rates, respectively (Figure IV-1-25). Unfortunately, as discussed above, at this time there are no reliable test measurements of k_d for gravel and cobble materials. In a riverine setting, current velocities are generally low enough that the hydraulic shear stress at the levee does not exceed τ_c for gravels and cobbles, so estimates of erosion rate are often not necessary to rule out erosion breach, avoiding the challenges estimating k_d .



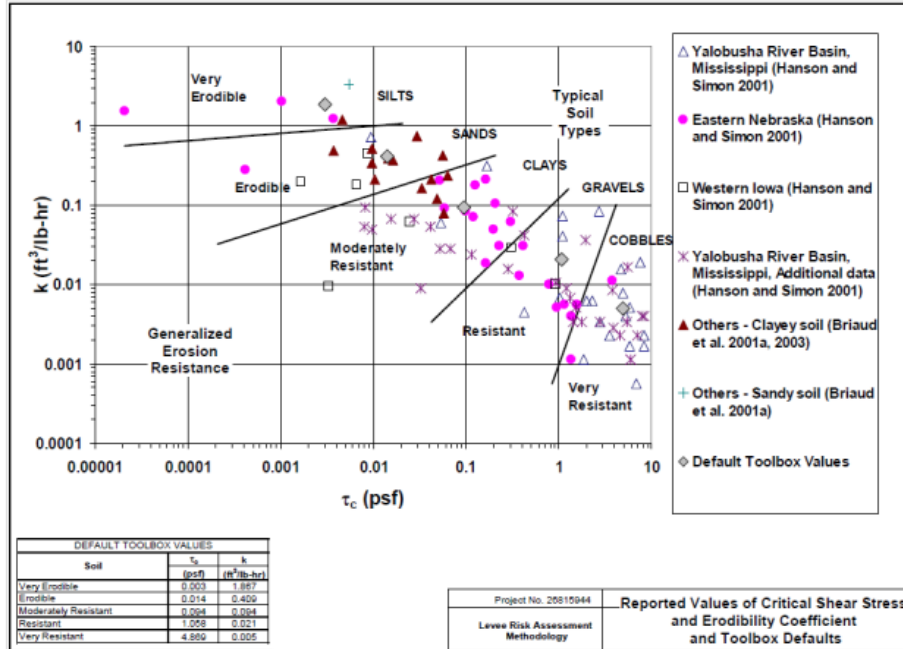


Figure IV-1-24 Reported Values of k_d and τ_c from JET and EFA tests performed by “Hanson” and “Briaud” on sand, silt, and clay soils, and Generalized Erosion Resistance categories from Hanson and Simon (2001). The table in the bottom left shows “Default” Risk Analysis Values for k_d and τ_c (URS 2007) for each erosion resistance category. Soil Type labels indicate typical USCS soil types associated with ranges of τ_c from Briaud (2008), but there is no data at this time that supports assigning k_d values to the non-cohesive soils. (URS 2007)

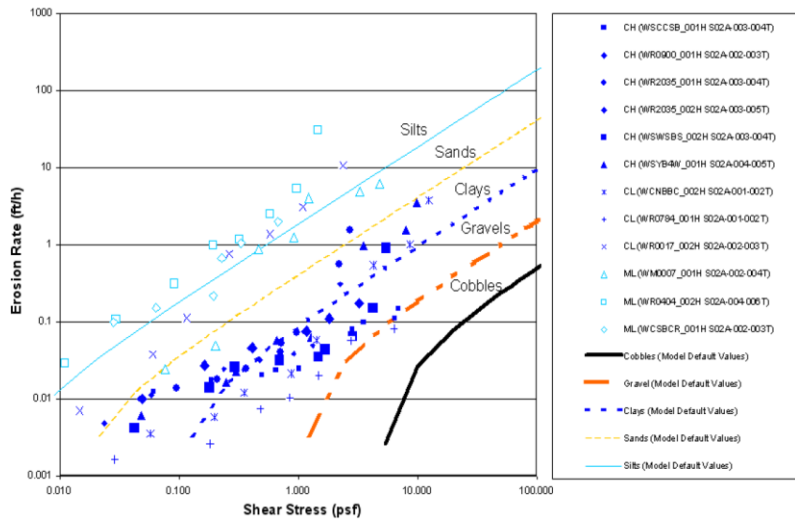


Figure IV-1-25 Measured versus Predicted Erosion Rates Based on “Default” values for k_d and τ_c as a function of Soil Classification/Plasticity used in the USACE Levee Erosion Risk Analysis Toolbox (Shewbridge et al, 2010). This figure shows only data from erosion rate tests of silt (ML) and clay soils (CL and CH). Lines for cohesionless soils (sands, gravels, cobbles) are speculative based on critical shear



stress values for those particle sizes (Briaud, 2008), but at this time there are no measurements of erosion rates for these materials.

Numerical Modeling Methods for the Erosion Process

There are multiple methods and tools that can be used to model and analyze the erosion process in rock and soils found in embankments and spillways. In many of these cases the methods were developed with a specific types of spillways and embankments, and then they have been adapted for use studying other types of embankments or spillways. User judgment will be required when applying these models to situations that vary from their original intent.

Spillway headcut erosion – SITES Model

The SITES model (<http://go.usa.gov/83z>) was developed by the U.S. Department of Agriculture (USDA) to simulate headcut erosion in earthen spillways. The model is based on laboratory studies and field observations of headcutting in soil and grass lined spillways. The computer program carries out a one-dimensional hydraulic simulation of flow through the spillway channel and evaluates the stability and integrity of the channel using a three-phase simulation of the headcutting erosion processes. Headcut erosion occurs in a variety of natural materials, especially when cohesion or other internal bonds hold the material together, or when there is a somewhat more erosion-resistant surface layer. Although the model was developed with a focus on soils, it has also been applied to rock channels.

The scope of the SITES model simulation is limited; the objective is to determine whether a headcut will form and whether the flow duration will be sufficient to deepen the headcut and cause it to advance upstream. If the erosion reaches the control sill of the spillway, the model concludes that the spillway has failed, and the run terminates. The simulation does not continue into the breach calculation phase since the spillway hydrograph was determined outside of the spillway erosion algorithm.

The three phases of the erosion process in a SITES simulation are as follows (Temple and Moore 1997):

1. Failure of vegetal cover and development of concentrated flow – Failure of vegetation can take place due to instantaneous total hydraulic stresses exceeding a threshold, or due to the time integral of erosionally effective stress exceeding a second threshold related to the plasticity index of the soil.
2. Downward erosion in the area of concentrated flow, leading to headcut formation – This phase is modeled using an excess stress equation with the soil characterized by a critical shear stress needed to initiate erosion and a detachment rate coefficient expressing the rate of erosion per unit of applied excess stress. For soil materials, the detachment rate coefficient, k_d , can be measured using laboratory or field submerged jet tests (Hanson and Cook 2004). Experience has shown that this is a crucial parameter affecting the performance of the SITES model. For rock materials, this parameter cannot be directly measured, and the SITES documentation suggests that a large detachment rate coefficient should be used.



- Continued downward erosion (which increases the headcut height) and upstream advance of the headcut – The advance rate is driven by the energy dissipation (stream power) at the headcut drop, and resistance is related to the headcut erodibility index, K_h . The index is used to establish the threshold for headcut movement and the rate of headcut advance.

Experience with the SITES model on rock spillway erosion problems (Wahl 2008a, 2008b) has shown that the detachment rate coefficient, k_d , is a crucial parameter affecting erosion predictions. Since this parameter cannot actually be measured for rock, a great deal of judgment is required to apply SITES to these situations.

Embankment breaching – WinDAM B model

WinDAM B is a dam breach simulation model that has been developed by the USDA, based on research conducted at the Agricultural Research Service hydraulics laboratory in Stillwater, Oklahoma. This software incorporates the SITES spillway erosion technology, and also allows the user to simulate breaching of homogeneous embankments from overtopping. WinDAM B is the second in a series of planned model developments.

- WinDAM A analyzed embankment overtopping only up to the point of imminent breach (breach initiation), and its output consisted only of a determination of whether breach occurred.
- WinDAM B analyzed breach development, with the breach caused only by overtopping flow
- WinDAM C will analyze breach development due to internal erosion (i.e., piping)
- Subsequent model versions are planned to incorporate capability for modeling zoned embankments.

For embankment overtopping, WinDAM B uses a similar phased erosion process as that employed in the SITES software, but emphasizes the breach development phase by separately considering headcut advance through different parts of the embankment. The four stages used by WinDAM B for embankment overtopping are:

1. Vegetal cover failure and headcut development
2. Headcut advance through the dam crest
3. Headcut advance into the reservoir (breach development)
4. Breach widening

The end of stage 2 marks the threshold for imminent breach or the end of the breach initiation process. Up to this point, intervention to save the dam may be possible (e.g., sandbags on crest, opening up additional spillway capability, etc.). Once stage 3 is entered, the flow rate increases dramatically; erosion causes the hydraulic control section to be enlarged, which allows an uncontrolled release of the reservoir storage.



WinDAM B includes practical features and capabilities that facilitate the dam breach simulation process. These include:

- routing of flows through the reservoir
- variable dam crest elevations (camber)
- multiple spillways
- flexible specification of inflow flood hydrograph

Although WinDAM B includes the spillway erosion modeling technology described for the SITES model, the level of output detail is not as great as SITES, so there may be situations in which users may still prefer the SITES model, which continues to be maintained by USDA. WinDAM B does have the capability to simulate embankment erosion and spillway erosion simultaneously, which permits it to be used to answer the question of which would occur first, a dam breach or spillway breach.

Differences between approaches to spillway erosion and embankment erosion in the WinDAM B and SITES models should be emphasized again. Both SITES and WinDAM B will simulate spillway headcut erosion only up to the point at which the most upstream headcut advances through the crest of the spillway (the high point of the spillway profile). For a spillway, they will not simulate the process of breach enlargement. For an embankment overtopping scenario, WinDAM B will simulate both breach initiation and breach development/enlargement. If a WinDAM B simulation includes both a spillway and an overtopped embankment and the spillway breaches first, you will not be able to draw any conclusions about what subsequently happens to the embankment. It is possible that the breach of the spillway could save the embankment, or if the breach process is slow, the embankment may continue to overtop and eventually fail. However, WinDAM B can only indicate which structure breaches first.

It should also be emphasized that the spillway erosion modeling performed by SITES and WinDAM B are intentionally conservative. The intent of these modeling tools was that they would be used for design, with the modeler adjusting a spillway design until no breach occurs. For this reason, the spillway erosion simulation conservatively estimates more erosion than is likely to occur in reality. In contrast, the embankment breach modeling capability in WinDAM was intended from the outset to be an analysis tool that would give an analyst the most accurate possible prediction of the outflow hydrograph produced by a potential breach.

Potential Failure Mode Event Tree for Spillway Erosion

When developing event trees during a potential failure mode analysis (PFMA) all of the steps previously mentioned in the erosion process may need to be included. In an event tree, each step would need to occur in order to fail a system by breaching the embankment from overtopping or failing the spillway due to headcutting. A possible sequence of events that can be used in a spillway erosion event tree is:



- Hydrologic event occurs and reservoir stage reaches the spillway crest.
- Spillway begins to flow.
- Vegetation is removed (if it is present).
- Concentrated flow erosion begins (downcutting forms headcut).
- Headcut advancement begins (Headcut deepens and advances towards spillway crest/control section).
- Intervention is unsuccessful.
- Headcut advances through crest of spillway and/or headcut undermines control structure/section and flow control is lost.
- Headcut advances into reservoir pool and breaching begins.

This possible event tree would be similar to one that would apply to embankment overtopping leading to a breach. A sample event tree for embankment overtopping is provided in the chapter on Flood Overtopping.

Relevant Case Histories

Gibson Dam: 1964

This case is described in the section on Dam Overtopping. Based on a detailed evaluation, the erodibility index of the dolomite abutment rock was estimated to be between 5,100 and 12,000 and the stream power was estimated to be between 43 kW/m² on the upper abutments and 258 kW/m² on the lower abutments. With these values, Figure 6 would predict about a probability of erosion of at most a few percent. In fact, very little erosion was observed.

Ricobayo Dam

Ricobayo Dam is a 320-foot high double-curvature arch dam constructed from 1929 to 1933 in Spain. The spillway at Ricobayo Dam is located on the left abutment of the dam and originally consisted of a 1300-foot long unlined channel at a slope of 0.0045 discharging over a rock cliff at the downstream end of the spillway. The design capacity of the spillway is 164,000 ft³/s. Flows through the spillway are regulated by four 68-foot by 35-foot gates. The rock in the spillway chute consisted of open-jointed granite.

Five separate scour events occurred along the spillway chute, with the first event occurring shortly after the dam was commissioned. Each of the flood events lasted over a period of several months, usually from December to June. From the initial major spill in January 1934, scour initiated and began progressing upstream. Attempts were made to stabilize the spillway chute after the flood events in 1934 and 1935. The vertical face of the drop at the downstream end of the chute and the right hand slope of the plunge pool were protected with concrete after the 1934 floods. Additional scour, about 80 feet downwards, occurred in the base of the plunge pool during the 1935 flood. After the 1935 flood, a concrete lip was added to the end of the spillway chute to direct flows further away from the face of the plunge pool drop. The concrete lip failed during the 1936 flood, as the plunge pool deepened another 100 feet, and the vertical face of the plunge pool experienced additional scour. During the 1939 flood event, the plunge pool did not deepen, but damage occurred at the vertical face of the plunge pool.



Even though the plunge pool did not deepen during the 1939 flood, measures were taken in the early 1940s to further stabilize the plunge pool. The plunge pool was lined with concrete, and concrete protection was added to the spillway channel and the drop at the end of the spillway channel. During 1962, the flood event reached a peak discharge of 170,000 ft³/s which caused failure of the plunge pool concrete lining that had been added in the 1940s. After the 1962 event, hydraulic splitters were added to the end of the spillway channel to break up the jet before it plunged into the pool. Since those modifications the spillway has passed floods with discharges ranging from 106,000 to 124,000 ft³/s without experiencing additional damage.

The Ricobayo spillway is located within a granite massif known as the Ricobayo Batholith. There are two prominent joint sets in the spillway foundation rock (joint sets A & B). Joint set A is generally vertically dipping. Joint set B is more horizontally dipping about 10-20 degrees. An anticline intersects the middle of the spillway at an angle of approximately 40°. Both joint set A and joint set B are relatively planar, but joint set B appears to be more continuous. Original speculation was that joints in the spillway foundation were clay filled and that this contributed to the scour during flood events. A site visit during 2005 indicated that the gouge was more likely rock flour and no clay was observed. Joint separation was generally less than 5 mm, with a maximum separation of 10 mm at some locations near the original surface. One additional feature in the spillway foundation is a near vertical fault that trends perpendicular to the spillway. The foundation rock adjacent to the fault has experienced intense shearing.

An evaluation of the scour that occurred over the years concluded that the geology in the spillway chute greatly contributed to the scour. To the right of the anticline axis, the scour progression was in the horizontal direction, while to the left of the anticline axis the scour progression was primarily in the vertical direction. The likely cause of the change in scour direction is the joint orientations on either side of the anticline axis. It was also believed that the fault in the channel played a role in the progression of the scour. The poorer quality of the rock along the fault allowed it to be easily eroded in a vertical direction. This is reflected in the erosion that occurred in 1935 (vertical scour of about 80 feet) and in 1936 (vertical scour of about 100 feet).

The plunge pool did not deepen during the flood event of 1939, indicating that the rock in the floor of the plunge pool was stronger than the rock that was eroded above it. This was also confirmed during the flood event in 1962. That flood event led to the destruction of the concrete lining in the plunge pool but no significant damage to the underlying rock. This led to the conclusion that the rock was stronger than the concrete lining provided to protect it.

A quantitative analysis of the plunge pool scour that occurred historically at Ricobayo Dam was performed, using the erodibility index method. The maximum scour depth is reached when the erosive power of the jet is less than the ability of the rock at the bottom of the plunge pool to resist it. Calculated and observed scour depths were compared (Annandale 2006). The calculated and observed scour depths from the 1935, 1936, and 1962 flood events generally were in good agreement. The analysis indicated that the calculations overestimated the scour that actually occurred in 1939, but that this was likely a function of much stronger erosion resistant rock at the base of the plunge pool after the 1936 flood.



Examples

Headcut Erodibility Index Calculation for Rock

You are at a site where there is a granite formation located immediately downstream of your spillway. Due to the weathered condition of the rock, there is concern that erosion could occur during a high discharge. You refer to the construction documents and the team geologist and have obtained the following information:

- The material of concern is granite with a uniaxial compressive strength of 20,000 psi.
- The rock quality designation is 50 percent.
- The material appears to be jointed in a four joint set.
- The joints are planar and smooth, with a tight joint separation, and the walls are slightly altered with sandy particles.
- The blocks appear to have a length to thickness ratio of 1:2 and the blocks dip downward into flow at 80 degrees.

Using this information and the tables in this chapter, what is the headcut erodibility index for the material?



References

- Annandale, G.W. 1995. Erodibility, *Journal Hydraulic Research, IAHR*, Vol. 33(4): 471-494.
- Annandale, George W. *Scour Technology – Mechanics and Engineering Practice*, McGraw-Hill Civil Engineering Series, First Edition, 2006, 430 pages.
- Barton, N., “Estimating the Shear Strength of Complex Discontinuities,” International Symposium on the Geotechnics of Structurally Complex Formations, vol. II, pp. 226-232, Capri, 1977.
- Briaud, J.-L., Ting F., Chen, H.C., Cao Y., Han S. -W., Kwak K. 2001. Erosion Function Apparatus for Scour Rate Predictions. *Journal of Geotechnical and Geoenvironmental Engineering*. ASCE, Vol. 127, N. 2, pp. 105-113.
- Briaud, J.-L., Chen, H.C., A.V. Govindasamy, and R. Storesund 2008 “Levee Erosion by Overtopping in New Orleans During the Katrina Hurricane” *J. Geotech. Geoenviron. Eng.* 2008.134:618-632.
- Briaud, J.-L., 2008, “Case Histories in Soil and Rock Erosion: Woodrow Wilson Bridge, Brazos River Meander, Normandy Cliffs, and New Orleans Levees”, The 9th Ralph B. Peck Lecture, *Journal of Geotechnical and Geoenvironmental Engineering*, Vol. 134, ASCE, Reston Virginia, USA.
- Bureau of Reclamation, *Erosion and Sedimentation Manual*, U.S. Department of the Interior, Bureau of Reclamation, Technical Service Center, Denver, Colorado, November 2006.
- Bollaert, E., “Transient Water Pressures in Joints and Formation Rock Scour due to High-Velocity Jet Impact,” Communication 13, Laboratoire de Constructions Hydrauliques Ecole Polytechnique Federale de Lausanne, Switzerland, 2002.
- Chow, V.T., *Handbook of Applied Hydrology*, McGraw-Hill Book Company. New York. 1964.
- Colorado Department of Transportation, Calculation of Bridge Scour Using the Erodibility Index Method, Annandale, G.; Smith, S.; March 2001.
- Ervine, D.A., et al, “Pressure Fluctuations on Plunge Pool Floors,” *Journal of Hydraulic Research*, Vol. 35, No. 2, pp. 257-279, 1997.
- Frizell, K.H, J.F. Ruff, and S. Mishra, “Simplified Design Guidelines for Riprap Subjected to Overtopping Flow,” Proceedings, ASDSO Annual Meeting, Las Vegas, Nevada, October 1998.
- Hanson, G. J., and A. Simon, 2001, “Erodibility of cohesive streambeds in the loess area of the midwestern USA” *Hydrol. Process.* 15, 23–38 (2001)



Hanson, G. J., and A. Simon, 2002, "Discussion of "Erosion Function Apparatus for Scour Rate Predictions" by J. L. Briaud, F. C. K. Ting, H. C. Chen, Y. Cao, S. W. Han, and K. W. Kwak" J. Geotech. Geoenviron. Eng. 2002.128:627-628.

Hanson, G. J., K.R. Cook, W. Hahn, and S. L. Britton, 2003, "Observed erosion processes during embankment overtopping tests." ASAE Paper No. 032066. ASAE St. Joseph, MI.

Hanson, G.G. and S. Hunt, 2007 "Lessons Learned Using Laboratory JET Method to Measure Soil Erodibility of Compacted Soils" Applied Engineering in Agriculture Vol. 23(3): 305-312

Hanson, G.J., and D. Temple, 2007, "Final Report on Coordination and Cooperation with the European Union on Embankment Failure Analysis" FEMA 602, 168p.

Hanson, G.J., T. Wahl, D. Temple, S. Hunt, and R. Tejral, 2010, "Erodibility Characteristics of Embankment Materials" Proceedings Association of State Dam Safety Officials Annual Conference

Hanson, G.J., D.M. Temple, S.L. Hunt, and R.D. Tejral, 2011, "Development and Characterization of Soil Material Parameters for Embankment Breach" Applied Engineering in Agriculture Vol. 27(4): 587-595

Kirsten, H.A.D., "A Classification System for Excavation in Natural Materials," the Civil Engineer in South Africa, pp. 292-308, July (Discussion in Vol. 25, No. 5, May 1983).

Mason, P.J., Arumugam, K., "Free Jet Scour below Dams and Flip Buckets." ASCE Journal of Hydraulic Engineering, Vol. 111, No. 2, 1985.

MacDonald, T.C., and Langridge-Monopolis, J., (1984). Breaching Characteristics of Dam Failures, Journal of Hydraulic Engineering, Vol. 110, No. 5, May, pgs 567-586

Moore, John S., Darrel M. Temple, and H.A.D. Kirsten, 1994, "Headcut Advance Threshold in Earth Spillways," *Bulletin of the Association of Engineering Geologists*, vol. XXXI, no. 2, June 1994, p. 277-280.

Morris, M.W., M.A.A.M. Hassan, T.L. Wahl, R.D. Tejral, G.J. Hanson, and D.M. Temple, 2012. Evaluation and development of physically-based embankment breach models. 2nd European Conference on Flood Risk Management, Nov. 20-22, 2012. Rotterdam, The Netherlands.

Scott, G.A., "Guidelines for Geotechnical Studies for Existing Concrete Dams," Bureau of Reclamation, Denver, Colorado, September 1999.

Shewbridge, S.E., Perri, J., Millet, R., Huang, W., Vargas, J., Inamine, M., Mahnke, S., (2010) "Levee Erosion Prediction Equations Calibrated with Laboratory Testing", Proc, V International Conference on Scour and Erosion, San Francisco, CA

Shields, A. (1936). "Anwendung der Aenlichkeitsmechanik und der Turbulenzforschung auf die Geschiebebewegung (Application of "similarity" mechanics and turbulence



research on the glacial movement.” Mittleilungen der Preussischen Versuchsanstalt fur Wasserbau und Schiffbau, W. P. Ott and J. C. Van Uchelen, translators, California Institute of Technology, Pasadena, Calif

Simon, A, R.E. Thomas, L. Klimetz, (2010) “Comparison and Experiences with Field Techniques to Measure Critical Shear Stress and Erodibility of Cohesive Deposits” Second Joint Federal interagency Conference, Las Vegas, NV

Temple, D., and Moore, J., 1997. Headcut advance prediction for earth spillways. *Transactions of the ASAE*, vol. 40, no. 3, p. 557-562.

URS. 2007. Erosion Toolbox: Levee Risk Assessment Methodology: Users Manual. Report prepared for the United States Army Corps of Engineers. 113p.

Veronese, A., “Erosioni de Fondo a Valle di uno Scarico.” *Annali dei avori Publicci*, Vol. 75, No. 9, pp. 717-726, Italy, 1937.

Wahl, T.L. 1998, “*Prediction of embankment dam breach parameters: A literature review and needs assessment*” DSO-98-004. Dam Safety Office, Water Resources Research Laboratory, U.S. Bureau of Reclamation. Denver, CO.

Wahl, T.L., 2008b. ***Modeling headcut erosion in a proposed fuse plug auxiliary spillway channel at Glendo Dam***, Hydraulic Laboratory Report HL-2008-05, U.S. Dept. of the Interior, Bureau of Reclamation, Denver, Colorado, 14 pp.

Wahl, T.L., 2008b. ***Stability analysis of proposed unlined spillway channel for Upper San Joaquin River Basin RM 274 embankment dam alternative***, Hydraulic Laboratory Report HL-2008-06, U.S. Dept. of the Interior, Bureau of Reclamation, Denver, Colorado, 28 pp.

Wahl, T.L. 2009 “Quantifying Erodibility of Embankment Materials for the Modeling of Dam Breach Processes” ASDSO Conference Proceedings

Wahl, T.L., 2014a, “Evaluation of Erodibility-Based Embankment Dam Breach Equations,” Hydraulic Laboratory Report HL-2014-02, U.S. Bureau of Reclamation

Wahl, T.L., 2014b “Measuring Erodibility of Gravelly Fine-Grained Soils” Hydraulic Laboratory Report HL-2014-05, U.S. Bureau of Reclamation

Wahl, T.L., 2015 Personal Communication

Wibowo, J.L., D.E. Yule, and E. Villanueva, “Earth and Rock Surface Spillway Erosion Risk Assessment,” Proceedings, 40th U.S. Symposium on Rock Mechanics, Anchorage Alaska, 2005.

Yildiz, D., Üzücek, E., “Prediction of Scour Depth from Free Falling Flip Bucket Jets”, Intl. Water Power and Dam Construction, November, 1994.



Xu, Y. and L.M. Zhang, 2009. Breaching parameters for earth and rockfill dams. *Journal of Geotechnical and Geoenvironmental Engineering*, 135(12):1957-1970.

IV-1-41



This Page Left Blank Intentionally

IV-1-42

